ELSEVIER

Contents lists available at ScienceDirect

Journal of Cleaner Production

journal homepage: www.elsevier.com/locate/jclepro





Understanding membrane-intensified catalytic CO₂ reduction reactions to methanol by structure-based multisite micro-kinetic model

Anže Prašnikar ^{a,**}, Mitja Linec ^a, Damjan Lašič Jurković ^a, David Bajec ^a, Marija Sarić ^b, Blaž Likozar ^{a,*}

ARTICLE INFO

Handling Editor: Xin Tong

Keywords:
Methanol
Hydrogen
CO₂
Membrane process intensification
Chemical reaction micro-kinetics
Catalysis surface structure

ABSTRACT

Membrane reactor processes can be used to overcome the constraints of the chemical rate equilibrium of methanol (MeOH) synthesis products. In this thermodynamics-limited work, three different selective sulfonated poly(ether ketones) (SPEEK) membranes were applied in an engineered unit operation with a commercial Cu/ ZnO/Al₂O₃/MgO surface catalyst for several CO₂/CO-involving chemistries. A detailed mathematical model with micro-kinetics was developed, optimised and utilised to assess the vessel with barrier by using CERRES (Chemical Reaction and Reactor Engineering Simulations). Scaled separation tests were described by the integrated reference values of permeance. The permeability for all compound molecules (H2, H2O, CO, CO2, MeOH) was determined by adjusting parameters to account for the experimental gas composition on the permeate, interface and retention segment side after reduction. The specific kinetic characteristics of the mechanism of elementary step reactions were analysed in fixed bed design. A comparison of the estimated data prediction for the packed system with related definite numbers showed excellent statistical agreement. Similarly, a very good reliability was obtained between the results for 3 SPEEK membrane cases. Thus, the defined particular evaluations of derived theoretical expressions were benchmarked accurately. Although (validated) performance, i.e. the yield of MeOH, was overestimated, discrepancy was not so large so as to simulate behaviour verily. The (3aminopropyl)triethoxysilane (polyamide) over a SPEEK layer performed best for intensification. Herein, the pressurised (>50 bar) CO2 hydrogenation pathway was not only shifted by in situ removal as a proof of concept, but also modelled intrinsically, considering transport phenomena resistances, adsorption and desorption as well. The storage of hydrogen can benefit from MeOH production reengineering.

1. Introduction

One of the most important and researched topics in the field of greenhouse gas emission reduction in recent decades is the conversion of the greenhouse gas CO_2 into useful chemicals to reduce the concentration of pollutants in the atmosphere and alleviate the pressure on fossil sources as a feedstock for bulk chemicals (Mustafa et al., 2020). Various processes are being considered, such as the two-step process in which synthesis gas is produced from CO_2 by dry reforming or reverse water-gas shift reaction, which is then converted into various chemicals (Schwab et al., 2015). An upgrade for process intensification is the one-step conversion of CO_2 into chemicals (Álvarez et al., 2017), especially methanol.

On paper, the reaction is relatively simple – hydrogen and CO_2 react to form methanol and water, usually in the gas phase in a heterogeneous catalytic reactor. However, the system is complicated by various side reactions, such as reverse water-gas shift (RWGS), and complex catalytic surface pathways. Numerous highly active catalyst formulations have been developed, such as Pd- (Bahruji et al., 2016) and Au-based (Hartadi et al., 2015) systems. However, the most studied and industrially relevant system remains the CuZnAl system (van den Berg et al., 2016; Günter et al., 2001; Prašnikar et al., 2022) due to its high performance, stability and low price. Operating conditions are carefully selected to maximise methanol yield – the process is usually carried out at 180–300 °C and relatively high pressures (above 20 bar) to achieve the desired thermodynamic equilibrium conversion and selectivity. Despite

E-mail addresses: anze.prasnikar@ki.si (A. Prašnikar), blaz.likozar@ki.si (B. Likozar).

https://doi.org/10.1016/j.jclepro.2024.142480

^a Department of Catalysis and Chemical Reaction Engineering, National Institute of Chemistry, Ljubljana, 1001, Slovenia

^b Energy & Materials Transition, TNO, Petten, 1755, Netherlands

^{*} Corresponding author.

^{**} Corresponding author.

numerous studies and excellent progress made in this field in recent decades (Jadhav et al., 2014), the process still falls short of its potential when it comes to widespread industrial use. One of the main reasons for this are the thermodynamic limitations (Álvarez et al., 2017).

A promising approach to overcome the thermodynamic limitations of single-pass yields is in situ separation in membrane reactors, where the products are continuously removed by permeation while the reagents remain in the reactive (catalytic) part of the reactor (Soltani et al., 1999). The concept has received much attention in petrochemistry (Takht Ravanchi et al., 2009) in processes such as steam reforming (Uemiya, 2004), water gas shift (Ma and Lund, 2003) and Fischer-Tropsch synthesis (Espinoza et al., 2000). For methanol synthesis, various studies have been carried out using zeolite (Gallucci et al., 2004; Seshimo et al., 2021; Van Tran et al., 2018), cation exchange (Struis et al., 1996) and polyimide (Lee et al., 2021) membranes. In addition to the use of membranes, a liquid sweep of high-boiling, methanol-absorbing tetraethylene glycol dimethyl ether was used to extract methanol across a hydrophobically modified alumina membrane (Li and Tsotsis, 2019). The key findings from the above studies are that different membrane types can be successfully used to exceed the equilibrium vield. The key aspects identified are membrane permeance, temperature-dependent selectivity of water over methanol and the reagents, and thermal and chemical stability. In addition to the membrane properties, the optimisation of the process parameters is extremely important for the process due to the complex interplay of various mass transfer phenomena. To find the optimal operating conditions and maximum product yield, a thorough understanding of the process is required to build an accurate model. At the heart of the reactor model is the reaction kinetics, which heavily depends on catalyst chemistry, surface morphology and particle size and shape. The Cu/ZnO/Al2O3 (CuZnAl), a ternary catalyst, exhibits considerable complexity and has been extensively studied by experimental (Sano et al., 2002; Lunkenbein et al., 2015; Hinrichsen et al., 2000; Chinchen et al., 1987; Schlebusch et al., 2012; Kattel et al., 2017) and theoretical ab initio methods (Schlebusch et al., 2012; Kuld et al., 2016; Tameh et al., 2018; Greeley et al., 2003). Although there is still some uncertainty about the exact active sites, surface mechanisms and kinetics, these studies have paved the way for the construction of complex microkinetic surface reaction models, one of the first on Cu(111) surface (Grabow and Mavrikakis, 2011). Such models are needed to cope with the complexity of surface reactions under a wide range of conditions and catalyst compositions, where ad hoc empirical models often fail.

In general, membrane properties, i.e. permeance and selectivity at different temperatures, pressures and gas compositions, can be determined by carefully designed experiments, allowing relatively accurate modelling of membrane mass transport. Nevertheless, the introduction of the membrane increases the complexity of the reactor model compared to a simple fixed-bed reactor. Coupling such models with full microkinetic surface models is non-trivial due to both system complexity and numerical considerations. Therefore, membrane models found in the literature are often coupled with simplified kinetics, where the reaction rates of the gas products are described with derived principal equations, trading accuracy for efficiency. Admittedly, many excellent membrane reactor models have been developed for processes such as methanol synthesis (Struis and Stucki, 2001; Samimi et al., 2017; Rahimpour and Ghader, 2003) and oxidative methane coupling (Esche et al., 2012; Barbieri et al., 2002), with some including fluid dynamics (Ountaksinkul et al., 2019) and heat balances (Shelepova et al., 2019). Nevertheless, there are opportunities for improvement. While Murmura et al. (2018) discuss improvements in mass and heat transport modelling, we would like to emphasise the importance of utilizing full surface microkinetic models to accurately describe the intricate complexity of MeOH synthesis on CuZnAl.

The aim of this work was to develop a detailed mathematical model for methanol synthesis in membrane reactors. For this purpose, experiments were carried out with three different membranes, firstly to determine the permeances and secondly to validate the mathematical model by comparing the experimental results obtained during methanol synthesis in the membrane reactor. A membrane reactor model with a spatial dimension that incorporates convective, diffusive and membrane mass transport was developed and efficiently coupled with a full microkinetic surface model within the CERRES software package (Jurković, 2020). This software is freely available for academic use and it can be used to describe other types of reactors (multiphase continuously stirred tank reactor, batch reactor, catalyst surface etc.). It is especially developed for a fast simulation of processes involving microkinetic reaction description. Here, the membrane model is coupled with a microkinetic CuZnAl surface model developed as a culmination of our previous studies (Prašnikar et al., 2019, 2021; Huš et al., 2017; Kopač et al., 2019; Pavlišič et al., 2020). In addition, thorough CO2 hydrogenation experiments were conducted with three different membranes to validate the model under a variety of experimental conditions and demonstrate the predictive power achieved by using an accurate surface model.

2. Experimental

The experimental part in this work consisted of three parts. In the first part, methanol synthesis was carried out in a fixed-bed reactor under different conditions. The data obtained were used for microkinetic modelling, in which kinetic parameters were determined that were used in the mathematical modelling of the membrane reactor. In the second part, the permeances of all three membranes were determined for all components. The values of the permeances and their dependence on temperature were needed for the mathematical model of the membrane reactor. A near-equilibrium composition of the feed with CO, CO2, H2, CH3OH and H2O was used. In the third part, methanol synthesis from CO, CO2 and H2 was carried out in the membrane reactor using different membranes. It was envisaged that the membrane reactor would be used after the fixed bed reactor to increase the methanol yield. Therefore, the feed to the reactor had a similar composition to that which would come from the fixed bed reactor - a thermodynamic equilibrium composition. The methanol yield and methanol flow rate obtained from the membrane reactor were compared with the developed mathematical model.

2.1. Membranes

3 different membranes with end caps and flange were selected for membrane reactor testing. The membranes were manufactured on a commercial extruded commercial α -alumina support tube (Inopor) with a pore size of about 4 μm , to which a series of intermediate layers of decreasing porosity and roughness were applied. Two layers were usually applied: an additional α -alumina layer with a pore size of 170–180 nm and a γ -Al $_2$ O $_3$ layer with a pore size of 3–4 nm (Bonekamp et al., 1996). The outer diameter of the membrane tubes was about 14 mm and the inner diameter about 10 mm. This support material was used for selective membrane layers. Microporous hybrid silica or polymer materials were deposited on the outside of the ceramic support to obtain a layer with the required membrane selectivity. The membranes were manufactured by the Netherlands Organisation for Applied Scientific Research (TNO). Fig. 1 shows a membrane assembly consisting of the membrane with end cap seal and a flanged inlet connection.



Fig. 1. Example of the membrane with seal and flange.

Two membranes with two different coating layers and one membrane with a mixed coating were prepared. In the first two membranes, the intermediate layer consisted of sulfonated polyether ether ketone (SPEEK). In previous tests, the SPEEK membrane showed useful permeances and higher selectivity values for methanol production compared to other polymer membranes. This layer of the membrane was shown to have preferential vapour permeation towards the reactive gases, especially hydrogen, under the conditions corresponding to the methanol synthesis reaction. The top layer over the SPEEK layer was made of (3-aminopropyl) triethoxysilane-(polyamide) (APTES-PA) (Paradis, 2012) for the first membrane and 1,2-bis(triethoxysilyl)ethane (BTESE) (Paradis, 2012) for the second membrane. APTES-PA and BTESE membranes were chosen because they have high gas retention properties. The third membrane had a hybrid coating layer combining SPEEK with polyimide (PI). All three membranes had a total length of 45.0 cm and an effective length of 17.9 cm. The inner diameter of the reactor was 24 mm and the outer and inner diameters of the membrane were 14 and 10 mm, respectively. The volume on the retentate side was 53.7 ml and on the permeate side 10.6 ml. The seals of the membranes were pressed onto the metal flange with a force of 105 N to fill the empty space between the membrane and the metal caps.

2.2. Reactor set-up

Both the membrane reactor and the membranes were built at TNO. The reactor consisted of an outer tube and an inner sweep tube separated by the membrane. It was designed for high operating pressures (100 bar) and high operating temperatures (300 $^{\circ}$ C). A thermocouple was placed centrally in the sweep tube and fixed with compression couplings. The membrane reactor was equipped with preheating coils, separator and evaporator and placed in a vertical customised furnace (Grelci Maras d. o.o.). The reactor with the heating coils, evaporator and separator was placed in a vertical furnace. The top and bottom of the furnace were closed to prevent the chimney effect. To achieve complete evaporation, the feed gas was passed through the preheating coils, the evaporator and the gas-liquid separator, which was monitored regularly to ensure that no liquid phase entered the membrane module. The module was protected from overpressure by a relief valve. The schematic of the reactor is shown in Fig. 2, while the schematic of the whole system is in Fig. S1.

The membrane reactor was designed to be filled with a catalyst on the outer/retentate side of the membrane. The feed was connected to the top of the reactor, while the retentate and permeate left the reactor at the bottom. A porous stainless-steel frit was used to prevent the catalyst from leaving the retentate tube. Helium was used as an internal standard to determine the gas flow rate of the outlets on both sides. A manual three-way valve was used to direct the He flow to either the retentate or permeate stream. Both were connected to the Micro GC Agilent 490 via an automatic valve so that the composition could be analysed. For more details about the reactor setup, see the supplementary information in Fig. S1. The pressure of both the retentate and permeate streams was controlled with backpressure regulators (Brooks SLA series).

The system was developed for a high-pressure test (80 bar). An HPLC pump (Beckman, 114M Solvent Delivery Module) was used to pump methanol and water to the evaporator, which ensured evaporation, mixing and heating of the liquid with the feed gas. The heating lines were kept at 350 °C to analyse water and methanol directly on the GC alongside the reactive gases. Since CO_2 is liquid at 80 bar and at room temperature, an HPLC pump with pump head cooling (Flusys, Wadose-Lite) was used to pump CO_2 and add it to the H_2 stream. The CO_2 evaporator, which mixes hydrogen and CO_2 , was heated to prevent freezing of the CO_2 inlet line. The H_2/CO_2 mixture was fed into the evaporator inside the furnace where H_2O and MeOH were added.

2.3. Membrane reactor and packed-bed reactor experiments

The catalytic experiments were carried out in both fixed-bed and

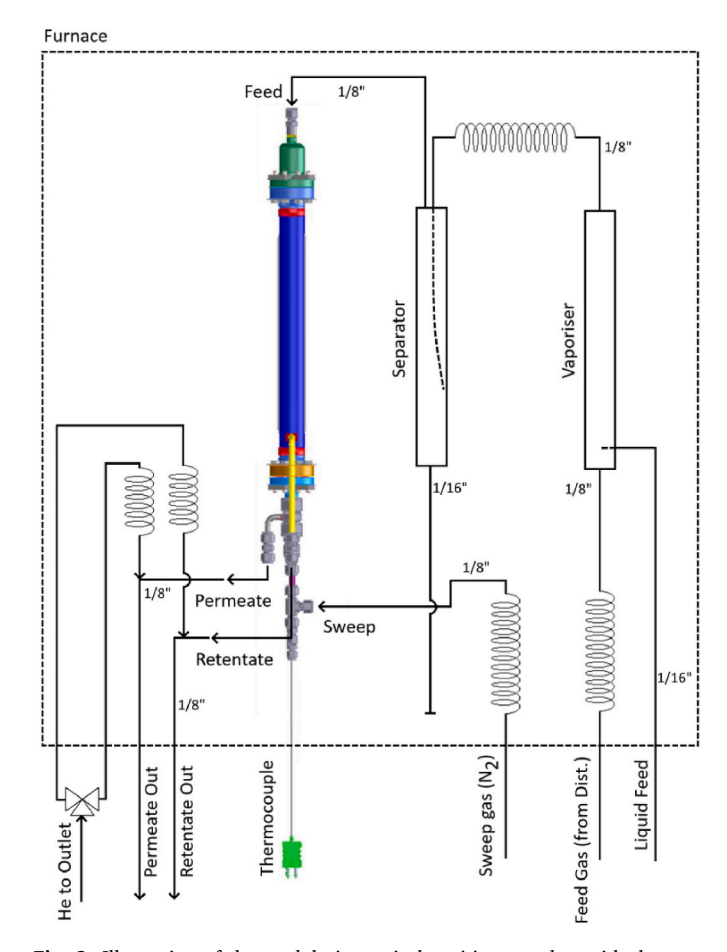


Fig. 2. Illustration of the module in vertical position together with the connecting elements inside the oven.

membrane reactors using a Cu/ZnO/Al $_2$ O $_3$ /MgO (CuZnAlMg) catalyst for methanol synthesis (Alfa Aesar). First, the kinetic parameters of the microkinetic model (Prašnikar et al., 2021) were adjusted based on the experimental data from the fixed-bed reactor. The kinetic parameters were then used to model the membrane reactor. The catalytic experiments in the membrane reactor were performed with the composition corresponding to the partially converted CO $_2$, i.e. the feed consisted of CO $_2$, CO, H $_2$ O, H $_2$ and MeOH. The composition used thus had a lower partial pressure of hydrogen and its permeation through the membrane was lower, so that a higher conversion of CO $_2$ in the membrane reactor could be achieved. In a real experimental plant, this could be achieved by first partially converting the CO $_2$ in a fixed bed reactor and then using the membrane reactor to overcome the thermodynamic equilibrium.

2.3.1. Packed-bed reactor experiments for microkinetic modelling

The set-up was described in detail in our earlier paper (Prašnikar et al., 2019). Briefly, the experiments were performed in a parallel packed bed reactor (tube diameter 6.35 mm) connected to a gas chromatograph (Agilent 490 Micro GC, TCD detectors equipped with CP-Molsieve and PoraPlot U-columns) via a heated line. A commercial catalyst from Alfa Aesar was used for the methanol synthesis. The composition of the catalyst is listed in Table 2. The gases used for the catalytic tests were pure $\rm H_2$ (99.999%, Messer), CO $_2$ (99.999%, Messer) and CO (99.999%, Messer). 0.209 g of the sieved catalyst with a particle size between 1 and 2 mm was used. The catalyst was first reduced in the reactor in a 3.0% $\rm H_2/N_2$ mixture at 250 °C. Experiments at 200, 220, 240, 250 and 260 °C were performed with a feed consisting of 75% $\rm H_2$ and 25% CO $_2$. Two experiments were conducted with a feed consisting of 69.8% $\rm H_2$, 7.5% CO $_2$ and 22.7% CO at 220 and 250 °C, respectively. The pressure was 20 bar and the weight hourly space velocity (WHSV)

was 33,300 Nml/(h g).

2.3.2. Experiments for the determination of membrane permeances

The permeances for each membrane were determined for each compound in the absence of the catalyst. After the membrane was installed in the membrane reactor, a high-pressure test was performed at room temperature. The feed pressure of N2 was set at 80 bar on the retentate side and the permeate pressure was in the range of 20-80 bar. After this test, the pressure was released and the membrane was heated to 250 $^{\circ}\text{C}$ at a heating rate of 0.5 K/min. The inlet pressure was then increased to 80 bar with a hydrogen stream and the permeate pressure was set to the lowest possible value for each membrane. The inlet was changed from H₂ to the appropriate composition and after steady state was reached, the composition of retentate and permeate was analysed. No sweep flow through the permeate side was used to achieve the highest possible transmembrane pressure (TMP) difference. The same procedure was used for experiments at 220 °C. The permeances were determined with the relevant composition close to the equilibrium composition for the feed with stoichiometric H₂/CO₂ ratio for isothermal MeOH synthesis at 250 °C and 80 bar as follows (Table 1).

This composition was used to simulate a realistic system consisting of a fixed-bed reactor and a membrane reactor in series. In this case, preconversion of the input gas in the fixed bed reactor would be used to minimise hydrogen loss through the membrane. The flow rate for the permeate composition was analysed and the permeances for all compounds and for each membrane were determined by adjusting the permeances in the mathematical model of the membrane reactor to match the experimentally determined composition on the permeate and retentate side. Other conditions are listed below. Two total flow rates (2 and 3 Nml/min) and two reactor temperatures (220 °C and 250 °C) were chosen, while the feed pressure was set at 80 bar. Due to the different permeances, the permeate pressure was set to 70 bar (BTESE); 50 bar (APTES-PA); 60 bar (SPEEK-PI).

2.3.3. Catalytic experiments in the membrane reactor

Catalytic experiments were carried out with APTES-PA and SPEEK-PI membranes at 220 $^{\circ}$ C and 250 $^{\circ}$ C. For the reaction with the BTESE membrane, the experiments for the catalytic process were not performed due to a problem with the reduction process. The same feed composition and pressures were used as for the experiments to determine the permeances at total flow rates of 2.0 and 3.0 Nl/min.

Since the permeant components were depleted to about 50%, the effect of concentration polarisation over the effective length of the membrane is estimated to be small. Due to the large permeate flow rate, it was also not necessary to use the sweep gas. The volume on the retentate side of the membrane was completely filled with 60 g of the catalyst to reduce catalyst movement and possible damage during installation or use of the membrane reactor. The catalyst was fixed inside the annulus by a ring of quartz wool on each side. The height of the catalyst bed was 16 cm and the void fraction of the bed was 0.49, the density of the catalyst was 2.44 g/ml.

An important step prior to the reaction was the activation of the catalyst, which had to be carried out very carefully to allow for the exothermic reduction of the catalyst. The procedure is described in the Supplementary in section 2. In general, the reduction process was

Table 1
Gas composition used to determine membrane permeances.

Gas	Composition, vol.%		
H ₂	65.1		
H_2O	7.7		
CO	3.3		
CO_2	19.5		
MeOH	4.4		

carried out at a total flow rate of 400 Nml/min and with 10 bar on the retentate side and 9 bar on the permeate side, and varying the temperature. In addition, the gas composition was measured to ensure that the reduction was complete.

2.4. Catalyst characterization

Thorough characterization of Alfa Aesar methanol synthesis catalyst, by using N $_2$ physisorption, XRD (X-ray powder diffraction), XPS (X-ray photoelectron microscopy), SEM-EDS (scanning electron microscopy coupled to energy dispersive spectroscopy) was performed. The samples were reduced at 250 °C for 2 h in $\rm H_2$ before analysis and then transferred in the inert atmosphere to glovebox for sample preparation for XRD and XPS analyses. The sample for XRD was covered using Kapton foil to prevent oxidation during transfer, while XPS sample was transferred to the instrument with special holder. A more detailed description about all techniques can be found in the Supplementary in section 3.

3. Theoretical

3.1. Mathematical model

The modelling was carried out with the software CERRES (Chemical Reaction and Reactor Engineering Simulations available at www.cerres. org), which was developed at the NIC. Fig. 3 shows a schematic of the membrane reactor. The feed is introduced into the system from the right side. The gases enter the outer ring of the module, then pass through the catalyst layer and exit on the left as retentate. Some of the gases enter the interior of the module through the membrane and exit through the permeate outlet.

For the membrane reactor model, the mass transport phenomena such as convection, diffusion and permeation through the membrane for each selected component were included, together with reaction phenomena such as adsorption and desorption of species on the catalytic surface along with catalytic surface microkinetic reactions. Reaction kinetics for the selected catalyst was separately measured in a packed-bed reactor and existing microkinetic model was adjusted through the regression analysis of kinetic parameters.

A membrane system consists of two volumes, the retentate (V_{ret}) and the permeate side (V_{perm}), which are separated by a membrane. Both sides are treated as separate systems with their own pressure, flow rate and gas concentrations at the inlet and outlet. The systems are coupled only by mass transfer across the membrane, which is limited to a certain number of species involved in the process. The mass transfer rate through the membrane for the coupled species is:

$$N_{memb.} = A_{memb.}P_i \left(p_{i,ret} - p_{i,perm} \right) = A_{memb.}P_iRT \left(c_{i,ret} - c_{i,perm} \right)$$
 (1)

where N_{memb} is the molar flow through the membrane in mol/s, A_{memb} the membrane surface area in m² and the P_i permeance of the species i in mol/(m² bar s). The mass balance for the gas component i in the retentate phase can be further described as follows:

$$\frac{\partial C_{i}}{\partial t} = -v_{x,ret} \frac{\partial C_{i}}{\partial x} + \frac{D_{i}}{\tau} \frac{\partial^{2} C_{i}}{\partial x^{2}} + C^{*} \frac{1 - \varepsilon}{\varepsilon} R_{i,cat} + R_{i,bulk} - \frac{N_{memb.}}{V_{ret} \ \varepsilon}$$
(2)

where the first term on the right-hand side of the equation represents mass transport with convection flow and ν_x gives the gas velocity in the axial direction. In all cases steady state solution was used $(\partial C_i/\partial t=0)$. The second term describes the diffusive/dispersive mass transport in the axial direction, where D_i is the diffusion coefficient and τ is the tortuosity factor due to a non-straight diffusion path through the catalytic bed. The third term represents the disappearance or formation of component i due to surface kinetics, multiplied in this case by the $R_{i,cat}$ expression where C^* is the concentrations of active sites per volume of catalyst and ε is the void fraction of the catalytic bed linking the changes in surface

 Table 2

 Characterization results of Alfa Aesar methanol synthesis catalyst.

	EDS composition ^a wt.%	XRD composition ^b wt.%	Crystallite size ^b , nm	Surf. phase composition XPS, % $^{\rm c}$ (mol.%) $^{\rm d}$	Unit cell size a, nm (CuZn alloy)
Cu	49 ± 5	76	8.1 ± 0.5	11 (8.2)	0.3618 (1.9%) ^f
ZnO	25 ± 2	16	5.3 ± 0.1	17 (10)	0.3252
Al_2O_3	13 ± 1	0.8 ^e		49 (32)	
MgO	1.8 ± 0.2			8 (6.3)	
С	12 ± 2	7 ^e		15 (18)	
BET m ² /g	66	Pore volume cm ³ /g	0.19	Cu area m²/g	7.3

- ^a Calculated from raw elemental composition to phase-based composition.
- ^b Based on Rietveld refinement of the crystalline part.
- ^c Surface phase composition, based on the same way of calculations as in our earlier work (Prašnikar et al., 2019).
- d Molar elemental composition of the cations and carbon (Cu, Zn, Al, Mg, Al), the missing part represents the molar fraction of oxygen.
- ^e Boehmite phase (AlO(OH)) and graphite phase detected.
- f Zn content in Cu based on Cu unit cell expansion correlation calculated as in our earlier work (Prašnikar et al., 2021).

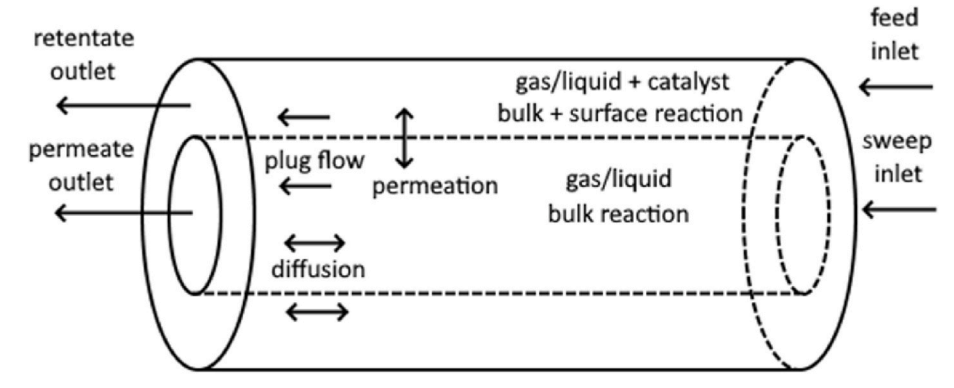


Fig. 3. The schematic representation of the membrane module.

coverage to changes in mass concentration of species. The fourth term defines the reaction term for the bulk-bulk reaction. The mass balance for the gas component i in the permeate phase is in line with the retentate phase:

$$\frac{\partial C_i}{\partial t} = -\nu_{x,perm} \frac{\partial C_i}{\partial x} + D_i \frac{\partial^2 C_i}{\partial x^2} + R_{i,bulk} + \frac{N_{memb.}}{V_{perm}}$$
(3)

The most important difference is that the second term describing the axial dispersion in the inner channel of the membrane does not include the tortuosity factor because there is no catalyst layer on the permeate side. The model boundaries involved constant molar flux at the entry and the exit of reactor along the length. The dispersion calculation can be found in our previous work (Prašnikar et al., 2022). To solve this system, the above equations are discretised so that they hold for a finite number of volumes and form a group of ordinary differential equations (ODEs). The gas velocity (v_x) in the permeate and retentate changes according to the molar balance of permeation and reaction. Only the changes in the radial direction are accounted, while the changes in the radial direction are neglected.

The reaction rate of the individual elementary reaction steps is represented by equation (4). Equation (5) describes the overall rate of consumption or generation of species.

$$r_n = k_{n,forward} \prod_{i=1}^{I} \theta_i^{S_{l,n,forward}} - k_{n,reverse} \prod_{i=1}^{I} \theta_i^{S_{j,n,reverse}}$$

$$\tag{4}$$

$$\frac{d\theta_i}{dt} = R_i = \sum_{n=1}^{N} \left(-S_{i,n,forward} + S_{i,n,reverse} \right) r_n \tag{5}$$

Here, r_n is the rate of the reaction numbered n and $k_{n,forward}$ and $k_{n,reverse}$ are the rate constants of the forward and reverse reactions respectively. The fraction of the active site covered by species i is denoted by θ_i . $S_{i,n}$,

forward and $S_{i,n,reverse}$ are the stoichiometric coefficients of species i in reaction n. The total number of reacting species is I and N is the total number of elementary reactions. The adsorption rates were calculated by multiplying the partial pressure of the adsorbing gas and the surface coverage of the empty active sites.

The proposed model was validated against experimental results in the membrane reactor and then used to find operating windows that are preferred for the membrane system. In this way, the modelling can provide information on membrane performance or on how to improve the reactor geometry. The net reactions considered in the microkinetic model for methanol synthesis are listed below. In addition to the methanol synthesis reaction, the reverse water-gas shift reaction was also included (r3). The mechanism consisted of 18 elementary reactions, which include reactions of adsorption/desorption and reactions on the surface of the catalyst. The reaction steps are listed together with the results in the Results section in Supplementary information (Table S1).

$$CO_2 + 3 H_2 \leftrightarrow CH_3OH + H_2O \tag{r1}$$

$$CO + 2 H_2 \leftrightarrow CH_3OH$$
 (r2)

$$CO_2 + H_2 \leftrightarrow CO + H_2O \tag{r3}$$

The permeance for each membrane was adjusted to the experimental values using a regression analysis. The temperature dependence of the permeance was modelled using the linear relationship where temperature in degrees Celsius is used:

$$P_i(T) = k_i T + n_i \tag{6}$$

Whereby k_i and n_i were adjustable parameters. The permeances were calculated from the logarithmic mean (see supplementary data, section 4) and used to adjust the parameters in the CERRES software (Jurković, 2020).

3.2. Effect of the catalyst composition on the activity

The most researched system for methanol synthesis is the Cu/ZnO/ Al₂O₃ system, in which Cu nanoparticles serve as the basis for CO₂ conversion. The copper itself does not efficiently hydrogenate the intermediates for methanol formation, so the ZnO is used as a promoter that stabilises the intermediates and provides higher reaction rates. This was observed in the single crystal study by Sano et al. (2002), where Cu (111) surfaces with different Zn coverages were characterised by XPS and evaluated for MeOH and CO synthesis. Due to the reduction of ZnO to Zn and the similar atomic size of Cu and Zn, the two are able to form a brass alloy (Prašnikar et al., 2021; Fujitani et al., 1997). The alloy itself acts as a system in which H2 activation occurs at the Cu sites and the Zn acts as a binding site for oxygen-containing species. The stable supply of hydrogen atoms from the copper to the intermediate at the Zn sites leads to its hydrogenation to methanol. The other compounds in the catalyst typically increase the number of active Cu and Zn sites, which increases its activity.

The ${\rm Al_2O_3}$ is a structural promoter of the catalyst that prevents the growth of Cu and ZnO nanoparticles (Prašnikar et al., 2019). On the longer range it is in the amorphous phase and covers around half of the catalyst surface as determined by the XPS. The amorphous layer of ${\rm Al_2O_3}$ is sensitive to the ${\rm H_2O}$ content in the gas phase, resulting in a loss of activity (Prašnikar et al., 2019).

Copper-zinc oxide-based catalyst promotes the conversion of CO_2 to MeOH and CO at the operating conditions, while MeOH synthesis from CO is negligible (Prašnikar et al., 2021). On the other hand, Alfa Aesar catalyst used herein also contains MgO. Cu/MgO is more active in MeOH synthesis from CO-H₂ mixture than from CO-CO₂-H₂ mixture (Studt et al., 2015). ZnO leads to a similar activity as in the case of the Cu/Z-nO/Al₂O₃ material, with the MeOH activity increasing with increasing CO₂ content in the CO-CO₂-H₂ mixture (Fujitani et al., 1997). It has also been observed that SrO, when involved, reacts immediately with CO₂ to form SrCO₃, which can be correlated with MgO since both are alkaline earth oxides. Zander et al. (2013) stated that Mg promotes the dispersion of Cu during catalyst synthesis as it has the same charge as Zn²⁺ and the size is only 2% different from Cu²⁺. Therefore, the nature of the active site is not changed by its presence in the reaction gas mixtures

containing CO_2 . The only effect of Mg is in the different number of active sites. For the above reasons, the microkinetic multisite model for methanol synthesis on the $Cu/ZnO/Al_2O_3$ sample was established based on the density functional theory calculation (DFT) for the Zn/Cu(211) structure (Prašnikar et al., 2021).

4. Results and discussion

4.1. CuZnAlMg catalyst characterization

In order to link the activity and the microkinetic model, structural properties of the catalyst under study had to be determined. In addition to Cu, ZnO and Al₂O₃, the catalyst of Alfa Aesar also contains about 1.8% MgO (Table 2). Despite the low content, XPS measurements show that the MgO phase accounts for 8% of the total catalyst surface, which was calculated using the molar fractions of the surface as in our previous work (Prašnikar et al., 2019). As already measured for HFW230 (Cu/ZnO/Al₂O₃, HiFuel W230, Alfa Aesar), the Al₂O₃ also accounts for half of the surface area (49%) and therefore probably contributes together with MgO to the increased thermal stability of the Cu and ZnO phases. The XRD results show that the two phases are mostly non-crystalline (at least in the range of the XRD measurements) and heterogeneously distributed over the catalyst, although we can find some particles containing both Al and Mg (SEM EDS mapping, Fig. 4), suggesting possible synergistic effects in terms of stability enhancement. In addition, also some carbon particles were observed that were present due to the graphite that was added as a binder.

From the shape of the XPS signal of Cu2p, it can be seen that Cu is still partially oxidised to Cu $^+$, which could be due to the presence of oxygen during the transfer. Nevertheless, the surface area is similar to our previous work where we combined the Cu surface area obtained from the pulsed N₂O surface oxidation with the Cu₂O surface area obtained by combining the XPS surface phase fraction and the total surface area of the catalyst determined by BET. In this case, a Cu₂O surface area of 7.3 m 2 /g was determined, whereas in our previous work with HFW230 (Prašnikar et al., 2019) it was 8.8 m 2 /g after reduction, leading to similar results. This is significant for determining the amount of active sites which is used in microkinetic modelling. Based on the observed

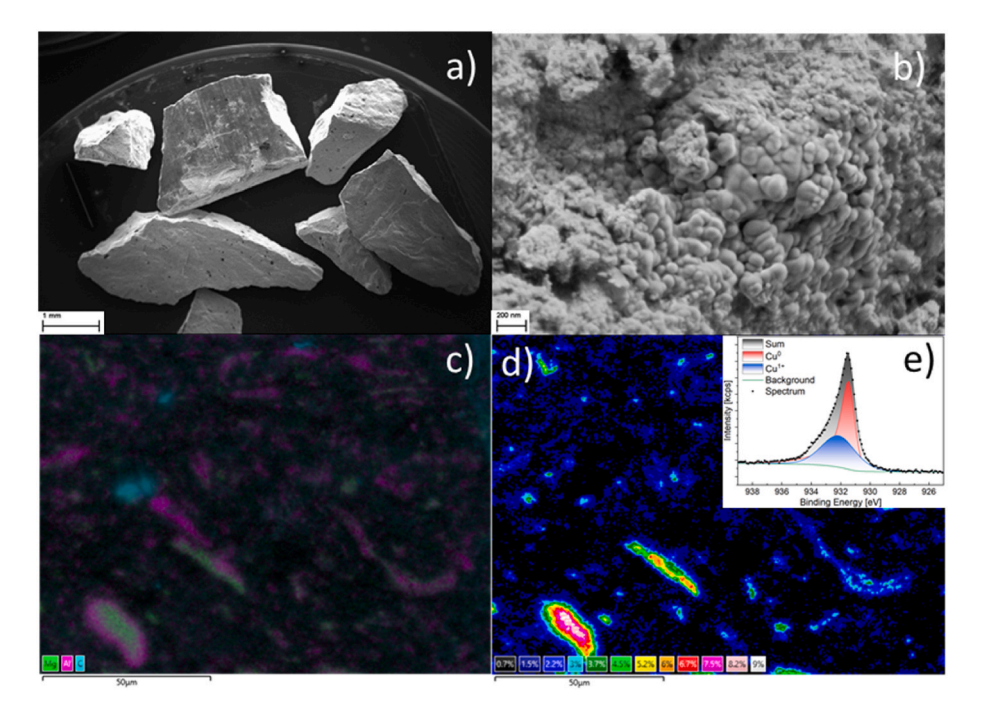


Fig. 4. a) SEM of 1 mm-2 mm catalyst particle fraction, b) SEM image of catalyst at a high magnification, c) SEM-EDS mapping of distribution of catalyst additives, d) Mg mass fraction distribution using SEM-EDS mapping, e) XPS of Cu 2p spectra showing presence of Cu¹⁺ and Cu⁰.

expansion of the Cu crystal unit cell, it can be concluded that a CuZn alloy (1.9% Zn in Cu) was formed after reduction, which is much smaller than in the case of reduction at 300 °C for 12 h (8.1% Zn in Cu) (Prašnikar et al., 2021), which could affect the number of active sites. In comparison, the a-parameter of the ZnO phase is almost the same as that from the library (measured: 0.3252 nm, JCPDS NO 80-0075: 0.3253 nm). The determined copper crystallite size is about 8 nm, which corresponds to the Cu size of the HFW230 catalyst. In general, the intrinsic activity (surface normalised) of Cu particles does not change above 8 nm (van den Berg et al., 2016). Additional characterization results can be found in supplementary, section 5. Overall, an activity similar to that of the HFW230 can be expected.

4.1.1. Microkinetic model for a packed-bed reactor

A list of the experiments with the reaction conditions and the outlet compositions obtained can be found in Table 3. For two of the conditions applied, the product mixture was close to equilibrium. In the regression of the kinetic parameters, the results of 5 experiments that were not near equilibrium were used.

In the microkinetic model, reactions at two types of active sites (Cu and Zn) were considered. Since the catalyst is similar to the Cu/ZnO/ Al₂O₃ (CuZnAl, HiFuel W230) catalyst based on characterization, the same concentration of active sites as for the mentioned catalyst (c_{Cu} = 0.2999 mol/L $_{cat},\,c_{Zn}=$ 0.0229 mol/L $_{cat})$ was used in the model. The kinetic parameters for CuZnAl from a previous work were used as a first estimate (Prašnikar et al., 2021). The original kinetic parameters are obtained from ab initio calculations presented in the work by Kattel et al. (2017). Surprisingly, it was found that active site concentration regression was not required and that the model could accurately predict the initial gas compositions when a CO₂-H₂ gas mixture was used. In the case of the H2-CO-CO2 mixture, the predicted MeOH formation was lower than observed experimentally. For this reason, the CO related kinetic parameters were optimised for the catalyst used. The adjustment was made by changing the activation energies or by changing the pre-exponential factors while maintaining the same ratio between forward and backward pre-exponential factors. This was done using the experimental points that were away from equilibrium and an excellent fit was obtained, as can be seen from Fig. S5 in the Supplementary Information, where the agreement of the model with the points away from equilibrium is shown. Since the parameters were changed without affecting the equilibrium, the final fit with the points of the equilibrium conversion obtained from the catalytic tests and the Gaseq Chemical Equilibrium programme (Morley, 2005) is excellent, as shown in Fig. 5.

The kinetic parameters for all elementary reaction steps involved are listed in supporting information (Table S1). The model with the obtained kinetic parameters was suitable for further mathematical modelling of the membrane reactor and the kinetic parameters and microkinetic model were used without further optimisation. In addition to the kinetics, it was necessary to determine the permeabilities of all gas species for all three membranes.

4.2. Determination of permeances in the experiments without catalyst

The permeances were first estimated using log-average pressure differences (Supporting information, section 4) and then inserted into the complete model and optimised. In experiments with the APTES-PA membrane, a slight excess of H₂O partial pressure in the permeate outlet was observed due to experimental error. To correct this, the H₂O permeance was adjusted to achieve a 5% lower partial pressure in the permeate than in the retentate, accounting for expected experimental error. This adjustment ensured the minimum partial pressure difference for water through the membrane. The comparison of experimental and model results for outlet mole fractions and total permeate fluxes is shown in Fig. S3 and Fig. S4, respectively, demonstrating agreement between model and experimental values. Permeance values and temperature coefficients are summarized in Table 4. Water exhibited the highest permeance, while MeOH was 5-6 times lower and comparable to hydrogen. CO₂ permeance was 2-3 times lower than H₂, and CO permeance was even smaller, about 1/5 of H₂. Due to the higher permeance of H₂ compared to MeOH, pre-conversion of H₂ to MeOH is desirable to limit H2 loss through the membrane. Selectivity calculations based on reactants (H₂ and CO₂) showed CO₂-based selectivity for H₂O around 17 and for MeOH about 3. Permeances increased with temperature for all components, while selectivities decreased. Fig. 6 illustrates selectivity dependence on temperature for APTES-PA membrane, with highest selectivity for water based on H2, decreasing rapidly with temperature. Methanol selectivity showed less significant decrease. CO2 selectivity remained less than 1 throughout 200-300 °C range, with permeance comparable to H2. CO2-based selectivities for H2O and CO2 increased with temperature, with H2O selectivity about 4 times greater than methanol. APTES-PA membrane appears suitable for methanol synthesis, facilitating efficient water removal and transfer to permeate side, potentially enhancing CO2 conversion and methanol yield, especially at lower temperatures where H2-based water selectivity is higher.

Comparisons between experimental and model results of SPEEK-PI for molecular fractions are shown in Fig. S5 and Fig. S6. The agreement confirms model validity and permeance values. Table 4 summarizes calculated values and coefficients for temperature-dependent permeances. Water exhibits the highest permeance (1.58·10⁻³ mol/(m² Pa h)), followed by MeOH (8.7·10⁻⁴ mol/(m² Pa h)). MeOH permeance slightly exceeds the one of hydrogen. MeOH selectivity based on CO2 permeance is about 2.9, while for water it is around 5.3, indicating SPEEK-PI membrane may not outperform APTES-PA. Permeances for reactants are higher compared to APTES-PA. Temperature has a minor impact on permeances, mainly affecting MeOH and H2. Selectivities based on H₂ and CO₂ permeances are depicted in Fig. 7. H₂O and MeOH selectivities based on H2 show similar temperature dependency, with H₂O being about 2 times greater. However, H₂O selectivity only reaches 2.75 at 200 °C, significantly lower than APTES-PA. MeOH and H2 selectivities are comparable, ranging from 1.7 to 0.8. CO2 selectivity is lower due to its lower permeance compared to H₂. SPEEK-PI membrane shows lower selectivities compared to APTES-PA.

For BTESE membrane, as in the case of APTES-PA membrane, the H_2O partial pressure in the permeate exceeded that in the retentate,

The conditions and results of the catalyst evaluation at P = 20 bar and a WHSV of 33,300 Nml/(h g).

T, °C	Inlet partial fract. , /			Outlet partial fract. , /					Close to equilibrium
	H_2	CO_2	CO	H_2	CO_2	CO	H ₂ O	CH ₃ OH	
260	0.75	0.25	0	0.716	0.205	0.030	0.039	0.010	Yes
250	0.75	0.25	0	0.720	0.214	0.023	0.033	0.010	Yes
240	0.75	0.25	0	0.726	0.221	0.016	0.026	0.010	No
220	0.75	0.25	0	0.736	0.235	0.006	0.015	0.008	No
200	0.75	0.25	0	0.743	0.242	0.002	0.008	0.005	No
250	0.698	0.075	0.227	0.682	0.073	0.222	0.005	0.018	No
220	0.698	0.075	0.227	0.687	0.073	0.229	0.004	0.008	No

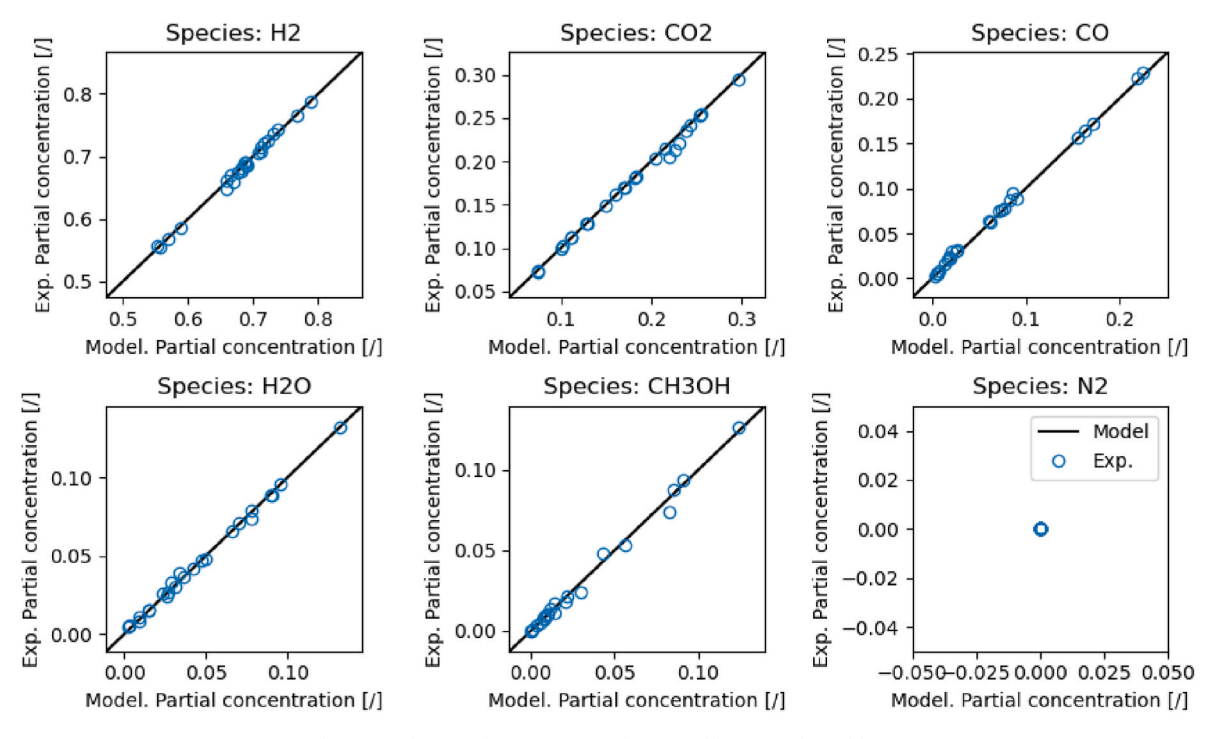


Fig. 5. The parity diagram for points away from equilibrium and equilibrium points.

Table 4Permeances of involved components at two temperatures and fitted coefficients in eq. (6) for all membranes.

Membrane	T, °C	Permeance, mol/(m ² Pa h)						
		$\overline{H_2}$	CO_2	CO	H ₂ O	МеОН		
APTES-PA	220	$2.24 \cdot 10^{-4}$	$9.87 \cdot 10^{-5}$	5.23·10 ⁻⁵	>1.67·10 ⁻³	$2.68 \cdot 10^{-4}$		
	250	$3.15 \cdot 10^{-4}$	$1.04 \cdot 10^{-4}$	$5.26 \cdot 10^{-5}$	$> 1.82 \cdot 10^{-3}$	$3.54 \cdot 10^{-4}$		
	k	$3.03 \cdot 10^{-6}$	$1.80 \cdot 10^{-7}$	$1.13 \cdot 10^{-8}$	$5.20 \cdot 10^{-6}$	$2.88 \cdot 10^{-6}$		
	n	$-4.43 \cdot 10^{-4}$	$5.91 \cdot 10^{-5}$	$4.98 \cdot 10^{-5}$	$5.21 \cdot 10^{-4}$	$-3.65 \cdot 10^{-4}$		
SPEEK-PI	220	$6.39 \cdot 10^{-4}$	$3.06 \cdot 10^{-4}$	$1.26 \cdot 10^{-4}$	$1.58 \cdot 10^{-3}$	$9.10 \cdot 10^{-4}$		
	250	$7.34 \cdot 10^{-4}$	$2.90 \cdot 10^{-4}$	$1.21 \cdot 10^{-4}$	$>1.58 \cdot 10^{-3}$	$8.30 \cdot 10^{-4}$		
	k	$3.14 \cdot 10^{-6}$	$-5.16 \cdot 10^{-7}$	$-1.49 \cdot 10^{-7}$	$2.35 \cdot 10^{-9}$	$-2.68 \cdot 10^{-6}$		
	n	$-5.16 \cdot 10^{-5}$	$4.19 \cdot 10^{-4}$	$1.58 \cdot 10^{-4}$	$1.58 \cdot 10^{-3}$	$1.50 \cdot 10^{-3}$		
BTESE	220	$3.24 \cdot 10^{-4}$	$1.32 \cdot 10^{-4}$	6.51·10 ⁻⁵	>6.61·10 ⁻⁴	$3.04 \cdot 10^{-4}$		
	250	$4.56 \cdot 10^{-4}$	$9.76 \cdot 10^{-5}$	$5.32 \cdot 10^{-5}$	$1.33 \cdot 10^{-3}$	$1.46 \cdot 10^{-4}$		
	k	$4.38 \cdot 10^{-6}$	$-1.14 \cdot 10^{-6}$	$-3.97 \cdot 10^{-7}$	$2.22 \cdot 10^{-5}$	$-5.28 \cdot 10^{-6}$		
	n	$-6.39 \cdot 10^{-4}$	$3.82 \cdot 10^{-4}$	$1.52 \cdot 10^{-4}$	$-4.23 \cdot 10^{-3}$	$1.47 \cdot 10^{-3}$		

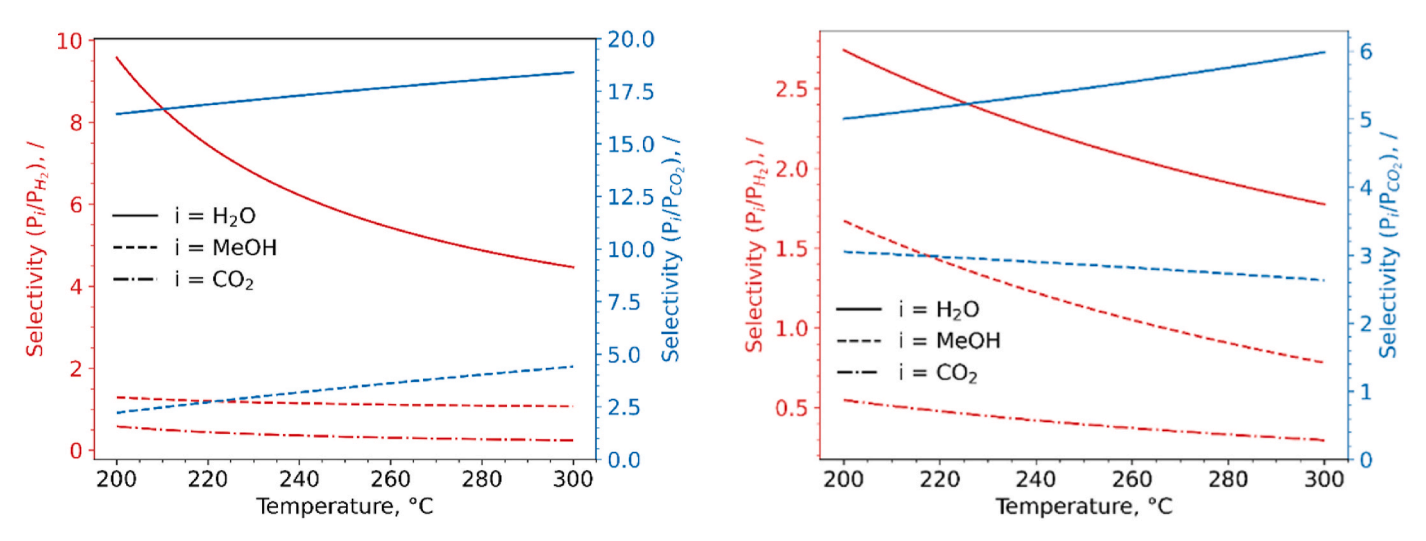


Fig. 6. Selectivities of APTES-PA membrane.

Fig. 7. Selectivities of SPEEK-PI membrane.

prompting an adjustment of the H₂O permeance to achieve a 5% lower partial pressure in the permeate. Comparisons between experimental and model results for outlet mole fractions and permeate flows are presented in Fig. S7 and Fig. S8, respectively, showing good agreement. Permeances and fitted coefficients are summarized in Table 4. Permeances are comparable to APTES-PA membrane, except for water, which is significantly lower. No clear trend is observed for permeances with increasing temperature. Water permeance, though the highest, is lower compared to previous membranes. Selectivity for H₂O ranges from 5.0 at 220 °C to 13.6 at 250 °C, with MeOH selectivity at 1.9. H_2O permeance is 2-3 times higher than that of hydrogen. Fig. 8 illustrates selectivity changes with temperature. Unlike previous membranes, H2based selectivity for water increases with temperature but does not reach APTES-PA levels. Methanol selectivity is comparable, but decreases rapidly with temperature. CO₂ selectivity remains similar to previous membranes. CO2-based selectivity shows a faster increase in H₂O selectivity with temperature, reaching about 60 at 300 °C, higher than other membranes, however at poor methanol selectivity.

The permeances of all relevant gasses are collected in Table 4. According to the results presented so far, the most suitable membrane among the three prepared and tested should be APTES-PA. Further experiments were conducted to validate the mathematical model and evaluate the performance of the membranes.

4.3. Catalytic experiments and membrane reactor model

The main series of experiments in the membrane reactor was carried out to investigate the enhancement of methanol production during the catalytic process of syngas conversion and the reverse water-gas shift reaction. It was found that the permeances increased with the service life due to the degradation of the membranes. Therefore, this change had to be considered when modelling the catalytic experiments in membrane reactors. Table 5 shows pressures on both sides of the membrane. The nitrogen flow rates for selected membranes were measured before and after all experiments had been carried out, but it was not possible to measure flow rates of more than 2 NI/min because the measuring range of the flowmeter was limited (Supporting information, Table S2).

Since the catalytic tests were performed before the permeance tests for the APTES-PA and SPEEK-PI membrane, all permeances, which was determined from the test without of the catalyst, were reduced by the appropriate factor (*F*) to obtain the model permeate flux rate equal to that measured from the catalytic experiments. The factor was optimised to obtain a good agreement between the experimental and model results. The list of factors obtained can be found in Table 5. In the case of BTESE, only the experiments to determine the permeance were

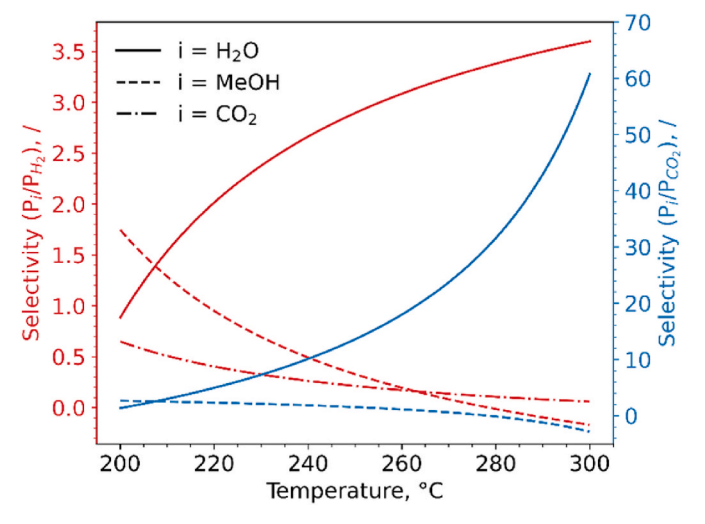


Fig. 8. Selectivities of BTESE membrane.

Table 5Testing conditions and factor F to adjust permeabilities for modelling catalytic MeOH production in a membrane reactor.

Membrane	p_{ret} bar	p_{perm} , bar	F	Exp. sequence
APTES-PA SPEEK-PI	80 80	50 60	0.64 0.48	Cat. → Perm. Cat. → Perm.
BTESE	80	70	1	Only perm.

performed.

4.3.1. APTES-PA membrane

In the experiments with the APTES-PA membrane, the highest TMP of 30 bar was maintained, with 80 bar on the retentate side and 50 bar on the permeate side. It was found that good agreement with the experimental results was obtained with the proposed mathematical model. The parity diagrams of the partial mole fractions for all components involved at all four conditions investigated are shown in Fig. S18. The experimental results for H₂, H₂O and MeOH agree very well with the model at all experimental conditions. The mean absolute percentage deviation (MAPD) for CO2 retentate and permeate is about 15%, the MAPD for CO retentate and CO permeate is 29% and 33%, respectively. The MAPD between the model and the experimental values for MeOH retentate is only 4%, but for MeOH permeate it is 18%. Considering that the mathematical model includes both the detailed microkinetics at the catalyst and the mass transfer across the membrane, the model describes the experimental data quite well and is suitable for modelling membrane reactors with APTES-PA membranes. Fig. S12 shows the comparison of the parity diagrams for the retentate and permeate outlet streams. The excellent agreement of the model with the experiments indicates that there was practically no accumulation of components within the membrane reactor and that the mass balances for the components were closed.

More detailed comparisons for the methanol volume flow rates achieved are shown by histograms in Fig. 10. The ratio between the mass of catalyst in the membrane reactor and the total volume flow rate (W/ φ) is used for the plot. For 60 g catalyst for each membrane, the W/φ ratio was 20 and 30 g min/l for 3.0 and 2.0 Nl/min total flow rate, respectively. From the histograms shown, it can be seen that a 10-20% higher methanol throughput can be obtained at 250 °C and a 5-10% higher value at 220 °C compared to the reaction without membrane. From the calculated results of the methanol flow rate for the model with and without membrane, the influence of the membrane on the increase in methanol production becomes clear. On average, the experimental values for the volumetric methanol permeate flux are 15% lower than the values predicted by the model. A higher deviation of 30% occurred at experimental conditions of 250 °C and a flow rate of 2.0 l/min. The fact that almost the entire initial feed stream permeated through the membrane under these conditions did not agree with the model prediction, leading to the final discrepancy. Furthermore, the combination of catalyst and membrane can increase the methanol permeate flow rate by about 20–40% compared to the inlet methanol flow rate. The lower improvement of 10% at 250 $^{\circ}$ C and 2.0 l/min feed flow rate can also be attributed to a higher total permeate flow rate at these experimental conditions.

The methanol yield (Y_{MeOH}), selectivity of MeOH (S_{MeOH}) and CO₂ conversion (X_{CO2}) definitions are given in supporting information (Section 11). The experimental and model yields with and without membrane are shown in Fig. S14. For comparison, a yield corresponding to the input composition that would be obtained in a fixed-bed reactor used before the membrane reactor in a realistic environment is also shown. Similar to the methanol flow rate (Fig. 9), the model prediction overestimates the influence of the membrane compared to the experimental data. The increase in yield predicted by the model compared to the model results without the membrane is similar to the increase in methanol flow rate in Fig. 9. The model predicts a greater improvement

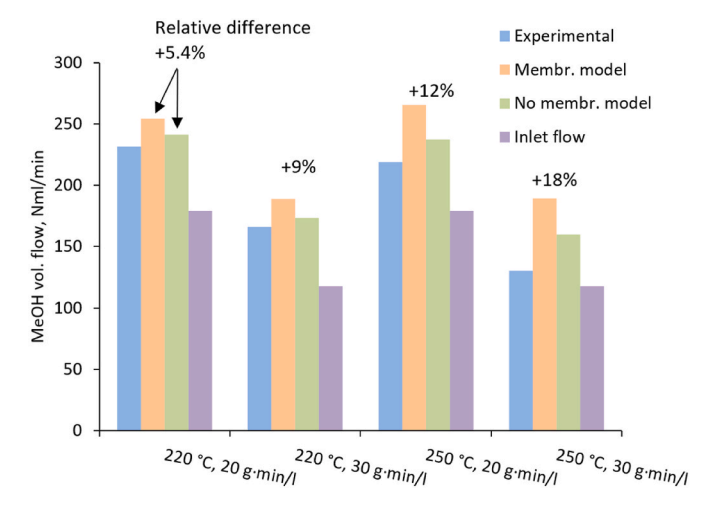


Fig. 9. Comparisons of MeOH permeate flows for catalytic tests with APTES-PA membrane.

at 250 °C than at 220 °C, although the $\rm H_2$ -based selectivity of the membrane for the products ($\rm H_2O$ and MeOH) decreases with temperature, while the $\rm CO_2$ -based selectivities increase with temperature. At 220 °C, a yield of about 30% of MeOH was obtained and almost no difference was observed between the two flow rates (20 and 30 g min/l), while at a higher temperature, the yield was still close to 30% at 20 g min/l, but dropped to 25% at 30 g min/l. Here the yield was not much better compared to the yield that would be obtained in a fixed bed reactor before the membrane reactor. In addition, a much larger discrepancy was observed between the predicted and experimental yields. This could be due to degradation of the membrane during the experiment, while also temperature variation and limitation of mass transport in axial direction could affect the system.

4.3.2. SPEEK-PI membrane

With the SPEEK-PI membrane, the highest TMP that could be maintained was 20 bar, with 80 bar on the retentate side and 60 bar on the permeate side. This is a 10 bar lower TMP than in the case of the APTES-PA membrane. The proposed model again shows good agreement with the experimental results, as can be seen from the parity plots (Fig. 10) of the partial mole fractions for all components involved at all four conditions. The values predicted by the model agree well with the experiments in the case of H2, CO2 and methanol. Here, the MAPD is only 4.1% for CO2 permeate and 11.2% for CO2 retentate. A similar deviation is observed for methanol, where the MAPD is 6.7% for MeOH retentate and 12.4% for MeOH permeate. A larger error was present in the case of CO. The permeate had a MAPD value of 43.6% and the retentate of 27.0%. Apart from this, the model is reasonably accurate and can be used to describe the membrane reactor. Fig. S13 shows the parity plot comparison for retentate and permeate outlet streams. The results again confirm a good description of the overall mass balance.

The calculations for the methanol volume flows and the MeOH yields obtained are shown as histograms in Fig. 11 and Fig. S15, respectively. From the results presented, it can be seen that the model predicts a 6–9% higher methanol flow rate at 250 °C and about 3-5% higher values at 220 °C compared to the model results without membrane. For all experimental conditions, less than 12% deviation is observed between the experimental and predicted values for the permeate methanol volumetric flow rate. Experimentally, about 40% higher CO2 conversions were obtained at 220 °C and about 20% higher conversions at 250 $^{\circ}$ C compared to the conversions at the inlet of the reactor. Since all reactions in the process are exothermic, it is expected that higher CO₂ conversion is achieved at lower temperatures. The conversion achieved is slightly better compared to the results with the APTES-PA membrane. The comparison of the results of the model with and without membrane shows that the calculations for the selective CO2 conversion again agree with the calculations of the MeOH permeate fluxes. The experimental results deviate from the model results by less than 15%, and the deviation is even smaller at 220 °C with less than 6%. At 250 °C, the difference is about 10-15%.

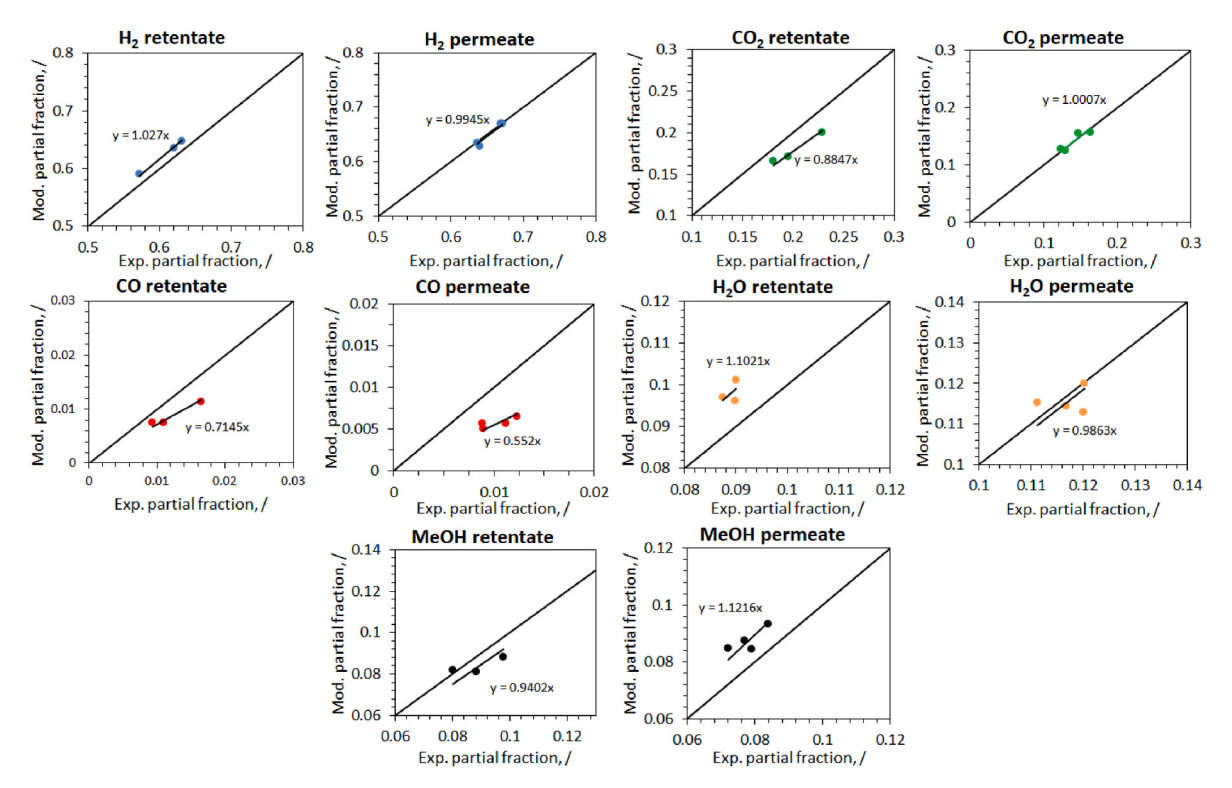


Fig. 10. Parity diagram of the partial fractions for catalytic tests with SPEEK-PI membrane.

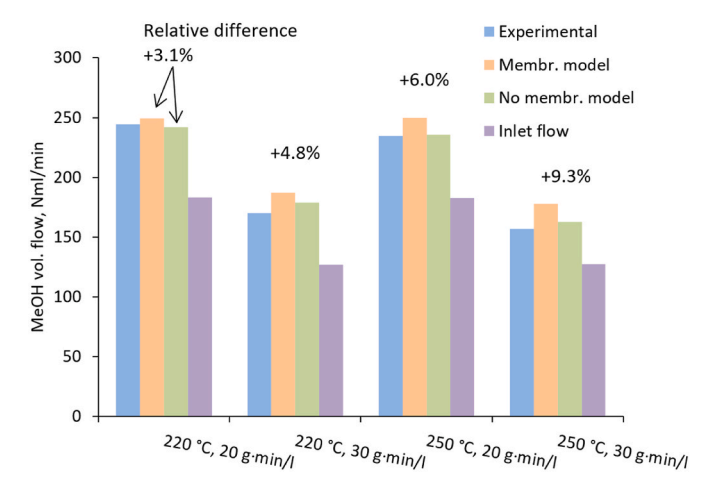


Fig. 11. Comparisons of MeOH permeate flows for catalytic tests with SPEEK-PI membrane.

The methanol yield is shown in Fig. S15. According to the model, a relatively small increase in yield can be obtained when the membrane is used at 220 °C. At a lower W/ ϕ the yield is 3.2% greater and at a higher W/ϕ the improvement is 4.8%. A greater effect of the membrane is observed at a higher temperature (250 $^{\circ}$ C), where a 9.4% improvement in yield can be obtained at 30 g min/l and at 20 g min/l the yield would be 6.1% better according to the model results. However, the overall difference between the model and experimental results is greater than this relatively small improvement in methanol yield predicted by the model. It is evident that the experimentally determined yield was greater at lower temperatures and that the values calculated by the mathematical model and the experimentally determined values are relatively close at this temperature. At higher temperatures, the difference between the model and the experimental results is greater and the model overestimates the yield in both cases, with and without the membrane.

4.3.3. BTESE membrane

For the BTESE membrane, the experiments for the catalytic process were not carried out because there was a problem with the reduction process. As this was the first membrane in line for catalytic testing, it was later found that a longer reduction time should be used during the first run. When the reaction process started in the membrane reactor, pure hydrogen was fed into the reactor to initially produce the desired pressures on the retentate and permeate sides. Soon after, a sharp rise in temperature up to 300 °C was observed inside the membrane reactor. Since the preparation of the reduced catalyst had not yet been completed, the final exothermic catalyst reduction during the main process led to the temperature rise. After the system had cooled down, the pressure test was performed again and it was found that the membrane was damaged due to the excessive temperature, as there was no transmembrane pressure difference between the two sides of the membrane.

Simulations were performed according to the proposed model, but the conditions used for the BTESE membrane during the permeability test were used. For the BTESE membrane this means the lowest TMP of 10 bar, with 80 bar on the retentate side and 70 bar on the permeate side. The evaluations for the methanol volume flows and CO₂ yields achieved are shown as histograms in Fig. S16 and Fig. S17, respectively. From the histograms shown, it can be seen that no significant increase in methanol flow rate and not even additional CO₂ conversion was achieved with the BTESE membrane at any temperature. This could clearly be due to a very low TMP and also the lower MeOH permeance values compared to the other two membranes.

4.3.4. Membrane performance comparison

The validated membrane reactor model is now used to simulate and compare the performance of membranes in a reactor with the same geometry as the catalytic tests. A low inlet and retentate pressure is chosen (35 bar) and a permeate pressure close to ambient (1.5 bar) to obtain a large relative pressure difference that allows more efficient product removal at a reasonable WHSV. The input gas (H₂/CO₂ = 3, input temperature = 230 °C) is pre-converted in an adiabatic reactor (product temperature 252 °C) and the composition is simulated with Gaseq. The membrane reactor model is isothermal and is set to 230 °C. The effect of inlet flow rate on CO₂ conversion and MeOH flow rate is shown in the following figures (Figs. 12 and 13).

It can be seen that the increase in performance is greatest at a low flow rate. However, the inlet flow rate is limited by the flow permeation through the membrane and is different for each membrane. It also appears that a very low inlet flux is not suitable as most of the flux is permeated and the gas-catalyst contact is very limited, hence the optimum in CO_2 conversion in the figure below. It appears that the APTES-PA membrane performs best, although the model uncertainty is large for this membrane.

5. Conclusions

The aim of this work was to develop a mathematical model including mass transfer including detailed microkinetics for methanol synthesis over commercial CuZnAlMg catalysts in a membrane reactor. The kinetic parameters were first taken from previous studies and adjusted according to the results of the reactions in a fixed bed reactor. Two active sites were considered. The microkinetic model results agree well with the experimental results in the fixed-bed reactor. The microkinetic model was then used for mathematical modelling of the membrane reactor, also taking into account mass transport through the membrane. The permeances of three different membranes were determined by optimising the permeance value in the mathematical model to match the gas composition on both sides of the membrane in the experiments where no catalyst was used. Excellent agreement of the model with the experimental values was obtained. Therefore, all the required parameters (permeances and kinetic parameters) used in the model were accurately determined. The results show that the developed mathematical model predicts the membrane reactor performance for the APTES-PA and SPEEK-PI membranes quite well and can be used to predict the performance or increase the methanol yield in industrial reactors. The mathematical model overestimated the methanol yield improvements for both membranes. This discrepancy between the

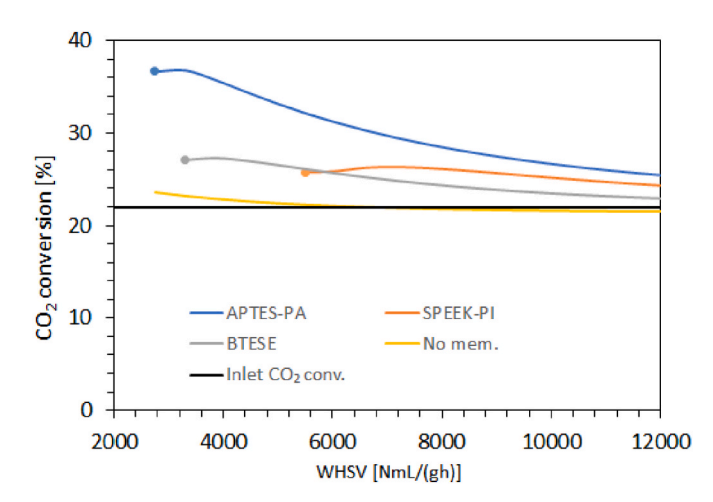


Fig. 12. CO $_2$ conversion simulation of the effect of inlet flow rate on mem. reactor performance at 35 bar (retentate), 1.5 bar (permeate), H $_2$ /CO $_2$ = 3, inlet T = 230 °C. The dots represent the points with 100% flow of the permeate.

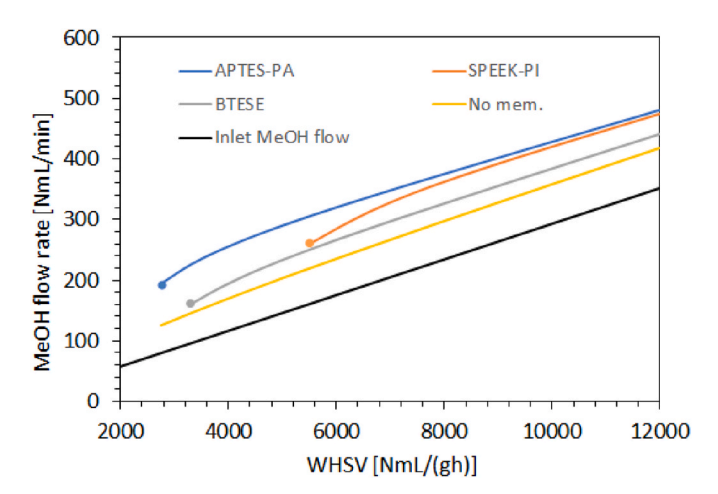


Fig. 13. Simulation of the effect of MeOH flow on the performance of the mem. reactor at 35 bar (retentate), 1.5 bar (permeate), $H_2/CO_2 = 3$, inlet $T = 230~^{\circ}C$. The dots represent the points of zero retentate flow-minimum inlet flow rate for stable operation at selected conditions.

model and the experiments can be explained by the gradual degradation of the membrane over time, while nonisothermicity and impact of axial mass transport limitation is not dismissed. It was observed that after conducting the experiments, the nitrogen flux through the membranes was greater than when they were first used. Nevertheless, the detailed microkinetic mathematical model developed in this work can be used to predict the behaviour of membrane reactors for methanol synthesis using APTES-PA, SPEEK-PI and BTESE membranes, for scale-up and optimisation of reactors, since the reaction mechanism, the kinetic parameters for elementary reactions and the permeances of the membranes have been accurately determined.

CRediT authorship contribution statement

Anže Prašnikar: Writing – original draft, Validation, Investigation, Formal analysis. Mitja Linec: Writing – original draft, Formal analysis. Damjan Lašič Jurković: Writing – original draft, Software, Methodology, Conceptualization. David Bajec: Writing – review & editing, Validation, Data curation. Marija Sarić: Writing – original draft, Investigation, Formal analysis, Conceptualization. Blaž Likozar: Writing – review & editing, Funding acquisition, Conceptualization.

Declaration of competing interest

The authors declare that they have no known competing financial interests or personal relationships that could have appeared to influence the work reported in this paper.

Data availability

Data will be made available on request.

Acknowledgments

The authors gratefully acknowledge the European Commission, as the work was established within the project Converge (Horizon 2020, grant agreement nr. 727504). The research was also supported by Slovenian Research and Innovation Agency (project UliSess nr. J7-4638, postdoctoral project nr. Z2-50049, research core funding nr. P2-0152). The authors acknowledge support from the Republic of Slovenia, Ministry of Higher Education, Science and Innovation, and from the European Union – NextGeneration EU in the framework of the project HyBReED, that is part of the Slovenian Recovery and Resilience Plan. Support of European Union (project HySTrAm, Horizon Europe, grant

agreement nr. 101058643) is gratefully acknowledged. The authors are highly thankful to Ajda Delić for N_2 physisorption measurements, Janvit Teržan for XPS measurements, Edi Kranjc for XRD measurements, Matic Grom for the help with reactor construction and operation and Matic Rode for preparation of an excellent graphical abstract.

Appendix A. Supplementary data

Supplementary data to this article can be found online at $\frac{https:}{doi.}$ org/10.1016/j.jclepro.2024.142480.

References

- Álvarez, A., Bansode, A., Urakawa, A., Bavykina, A.V., Wezendonk, T.A., Makkee, M., Gascon, J., Kapteijn, F., 2017. Challenges in the greener production of formates/ formic acid, methanol, and DME by heterogeneously catalyzed CO2 hydrogenation processes. Chem. Rev. 117, 9804–9838. https://doi.org/10.1021/acs. chemrey 6h00816
- Bahruji, H., Bowker, M., Hutchings, G., Dimitratos, N., Wells, P., Gibson, E., Jones, W., Brookes, C., Morgan, D., Lalev, G., 2016. Pd/ZnO catalysts for direct CO2 hydrogenation to methanol. J. Catal. 343, 133–146. https://doi.org/10.1016/j. jcat.2016.03.017.
- Barbieri, G., Marigliano, G., Golemme, G., Drioli, E., 2002. Simulation of CO₂ hydrogenation with CH₃OH removal in a zeolite membrane reactor. Chem. Eng. J. 85, 53–59
- Bonekamp, B.C., 1996. Chapter 6 Preparation of asymmetric ceramic membrane supports by dip-coating. In: Burggraaf, A.J., M.S, L.B.T., Cot, T. (Eds.), Fundam. Inorg. Membr. Sci. Technol. Elsevier, pp. 141–225. https://doi.org/10.1016/S0927-5193 (96)80009-X
- Chinchen, G.C., Denny, P.J., Parker, D.G., Spencer, M.S., Whan, D.A., 1987. Mechanism of methanol synthesis from CO2/CO/H2 mixtures over copper/zinc oxide/alumina catalysts: use of 14C-labelled reactants. Appl. Catal. 30, 333–338. https://doi.org/ 10.1016/S0166-9834(00)84123-8.
- Esche, E., Arellano-Garcia, H., Biegler, L.T., Wozny, G., 2012. Two-dimensional modeling of a packed-bed membrane reactor for the oxidative coupling of methane. Chem. Eng. Trans. 29, 1537–1542. https://doi.org/10.3303/CET1229257.
- Espinoza, R.L., Du Toit, E., Santamaria, J., Menendez, M., Coronas, J., Irusta, S., 2000. Use of membranes in Fischer-Tropsch reactors. Stud. Surf. Sci. Catal. 130 A, 389–394. https://doi.org/10.1016/s0167-2991(00)80988-x.
- Fujitani, T., Matsuda, T., Kushida, Y., Ogihara, S., Uchijima, T., Nakamura, J., 1997. Creation of the active site for methanol synthesis on a Cu/SiO2 catalyst. Catal. Lett. 49, 175–179. https://doi.org/10.1023/A:1019069708459.
- Gallucci, F., Paturzo, L., Basile, A., 2004. An experimental study of CO2 hydrogenation into methanol involving a zeolite membrane reactor. Chem. Eng. Process. Process Intensif. 43, 1029–1036. https://doi.org/10.1016/j.cep.2003.10.005.
- Grabow, L.C., Mavrikakis, M., 2011. Mechanism of methanol synthesis on Cu through CO2 and CO hydrogenation. ACS Catal. 1, 365–384. https://doi.org/10.1021/
- Greeley, J., Gokhale, A.A., Kreuser, J., Dumesic, J.A., Topsøe, H., Topsøe, N.Y., Mavrikakis, M., 2003. CO vibrational frequencies on methanol synthesis catalysts: a DFT study. J. Catal. 213, 63–72. https://doi.org/10.1016/S0021-9517(02)00040-4.
- Günter, M.M., Ressler, T., Bems, B., Büscher, C., Genger, T., Hinrichsen, O., Muhler, M., Schlögl, R., 2001. Implication of the microstructure of binary Cu/ZnO catalysts for their catalytic activity in methanol synthesis. Catal. Lett. 71, 37–44. https://doi.org/ 10.1023/4:1016696022840.
- Hartadi, Y., Widmann, D., Behm, R.J., 2015. CO2 hydrogenation to methanol on supported Au catalysts under moderate reaction conditions: support and particle size effects. ChemSusChem 8, 456–465. https://doi.org/10.1002/cssc.201402645.
- Hinrichsen, O., Genger, T., Muhler, M., 2000. Probing the elementary steps of the water-gas shift reaction over Cu/ZnO/Al2O3 with transient experiments. Stud. Surf. Sci. Catal. 130 D, 3825–3830. https://doi.org/10.1016/s0167-2991(00)80619-9.
- Huš, M., Kopač, D., Strah Štefančič, N., Lašič Jurković, D., Dasireddy, V.D.B.C., Likozar, B., 2017. Unravelling the mechanisms of CO2 hydrogenation to methanol on Cu-based catalysts using first-principles multiscale modelling and experiments. Catal. Sci. Technol. 7, 5900–5913. https://doi.org/10.1039/c7cy01659j.
- Jadhav, S.G., Vaidya, P.D., Bhanage, B.M., Joshi, J.B., 2014. Catalytic carbon dioxide hydrogenation to methanol: a review of recent studies. Chem. Eng. Res. Des. 92, 2557–2567. https://doi.org/10.1016/j.cherd.2014.03.005.
- Jurković, D.L., 2020. CERRES Chemical Reaction and Reactor Engineering Simulations.
 Kattel, S., Ramirez, P.J., Chen, J.G., Rodriguez, J.A., Liu, P., Ramírez, P.J., Chen, J.G., Rodriguez, J.A., Liu, P., 2017. Active sites for CO2 hydrogenation to methanol on Cu/ZnO catalysts. Science 355, 1296–1299. https://doi.org/10.1126/science.aal3573
- Kopač, D., Likozar, B., Huš, M., 2019. Catalysis of material surface defects: multiscale modeling of methanol synthesis by CO2 reduction on copper. Appl. Surf. Sci. 497 https://doi.org/10.1016/j.apsusc.2019.143783.
- Kuld, S., Thorhauge, M., Falsig, H., Elkjær, C.F., Helveg, S., Chorkendorff, I., Sehested, J., Sebastian Kuld, J.S., Thorhauge, Max, Falsig, Hanne, Elkjær, Christian F., Helveg, Stig, Ib Chorkendorff, 1, Kuld, S., Thorhauge, M., Falsig, H., Elkjær, C.F., Helveg, S., Chorkendorff, I., Sehested, J., 2016. Quantifying the promotion of Cu catalysts by ZnO for methanol. Science 352, 969–974. https://doi.org/10.1002/ 9783527610044.hetcat0148.

- Lee, J., Park, H.G., Hyeon, M.H., Kim, B.G., Kim, S.K., Moon, S.Y., 2021. Low-temperature CO2 hydrogenation overcoming equilibrium limitations with polyimide hollow fiber membrane reactor. Chem. Eng. J. 403, 126457 https://doi.org/10.1016/j.cej.2020.126457.
- Li, Z., Tsotsis, T.T., 2019. Methanol synthesis in a high-pressure membrane reactor with liquid sweep. J. Membr. Sci. 570–571, 103–111. https://doi.org/10.1016/j. memsci.2018.09.071.
- Lunkenbein, T., Schumann, J., Behrens, M., Schlogl, R., Willinger, M.G., 2015. Formation of a ZnO overlayer in industrial Cu/ZnO/Al2O3 catalysts induced by strong metal support interactions. Angew. Chem. Int. Ed. 54, 4544–4548. https://doi.org/10.1002/anie.201411581.
- Ma, D., Lund, C.R.F., 2003. Assessing high-temperature water-gas shift membrane reactors. Ind. Eng. Chem. Res. 42, 711–717. https://doi.org/10.1021/ie020679a. Morley, C., 2005. Gaseq - A Chemical Equilibrium Program for Windows.
- Murmura, M.A., Cerbelli, S., Annesini, M.C., 2018. Modeling fixed bed membrane reactors for hydrogen production through steam reforming reactions: a critical analysis. Membranes 8. https://doi.org/10.3390/membranes8020034.
- Mustafa, A., Lougou, B.G., Shuai, Y., Wang, Z., Tan, H., 2020. Current technology development for CO2 utilization into solar fuels and chemicals: a review. J. Energy Chem. 49, 96–123. https://doi.org/10.1016/j.jechem.2020.01.023.
- Ountaksinkul, K., Vas-Umnuay, P., Kasempremchit, N., Bumroongsakulsawat, P., Kim-Lohsoontorn, P., Jiwanuruk, T., Assabumrungrat, S., 2019. Performance comparison of different membrane reactors for combined methanol synthesis and biogas upgrading. Chem. Eng. Process. Process Intensif. 136, 191–200. https://doi.org/10.1016/j.cep.2019.01.009.
- Paradis, G.G., 2012. Novel Concepts for Microporous Hybrid Silica Membranes. University of Twente. https://doi.org/10.3990/1.9789036533669.
- Pavlišić, A., Huš, M., Prašnikar, A., Likozar, B., 2020. Multiscale modelling of CO2 reduction to methanol over industrial Cu/ZnO/Al2O3 heterogeneous catalyst: linking ab initio surface reaction kinetics with reactor fluid dynamics. J. Clean. Prod. 275 https://doi.org/10.1016/j.jclepro.2020.122958.
- Prašnikar, A., Pavlišič, A., Ruiz-Zepeda, F., Kovač, J., Likozar, B., 2019. Mechanisms of copper-based catalyst deactivation during CO2 reduction to methanol. Ind. Eng. Chem. Res. 58, 13021–13029. https://doi.org/10.1021/acs.iecr.9b01898.
- Prašnikar, A., Jurković, D.L., Likozar, B., Lašič Jurković, D., Likozar, B., 2021. Reaction path analysis of CO2 reduction to methanol through multisite microkinetic modelling over Cu/ZnO/Al2O3 catalysts. Appl. Catal. B Environ. 292, 120190 https://doi.org/10.1016/j.apcatb.2021.120190.
- Prašnikar, A., Dasireddy, V.D.B.C., Likozar, B., 2022. Scalable combustion synthesis of copper-based perovskite catalysts for CO2 reduction to methanol: reaction structure–activity relationships, kinetics and stability. Chem. Eng. Sci. 250, 117423.
- Rahimpour, M.R., Ghader, S., 2003. Theoretical investigation of a Pd-membrane reactor for methanol synthesis. Chem. Eng. Technol. 26, 902–907. https://doi.org/10.1002/ ceat.200301717
- Samimi, F., Rahimpour, M.R., Shariati, A., 2017. Development of an efficient methanol production process for direct CO2 hydrogenation over a Cu/Zno/Al2O3 catalyst. Catalysts 7. https://doi.org/10.3390/catal/7110332.
- Sano, M., Adaniya, T., Fujitani, T., Nakamura, J., 2002. Oxidation of a Zn-deposited Cu(1 1 1) surface studied by XPS and STM. Surf. Sci. 514, 261–266. https://doi.org/10.1016/S0039-6028(02)01639-4.

- Schlebusch, C.M., Skoglund, P., Sjödin, P., Gattepaille, L.M., Hernandez, D., Jay, F., Li, S., De Jongh, M., Singleton, A., Blum, M.G.B., Soodyall, H., Jakobsson, M., 2012. The active site of methanol synthesis over Cu/ZnO/Al2O3 industrial catalysts. Science 1187
- Schwab, E., Milanov, A., Schunk, S.A., Behrens, A., Schödel, N., 2015. Dry reforming and reverse water gas shift: alternatives for syngas production? Chem.-Ing.-Tech. 87, 347–353. https://doi.org/10.1002/cite.201400111.
- Seshimo, M., Liu, B., Lee, H.R., Yogo, K., Yamaguchi, Y., Shigaki, N., Mogi, Y., Kita, H., Nakao, S., 2021. Membrane reactor for methanol synthesis using Si-rich LTA zeolite membrane. Membranes 11, 1–9. https://doi.org/10.3390/membranes11070505.
- Shelepova, E.V., Ilina, L.Y., Vedyagin, A.A., 2019. Mathematical modeling of a catalytic membrane reactor: dehydrogenation of methanol over copper on silicamontmorillonite composite. React. Kinet. Mech. Catal. 127, 117–135. https://doi. org/10.1007/s11144-019-01567-z.
- Soltani, S., Sahimi, M., Tsotsis, T., 1999. Catalytic membrane reactors. Membr. Technol. 1999, 5. https://doi.org/10.1016/s0958-2118(99)90370-1.
- Struis, R.P.W.J., Stucki, S., 2001. Verification of the membrane reactor concept for the methanol synthesis. Appl. Catal. Gen. 216, 117–129. https://doi.org/10.1016/ S0926-860X(01)00548-8.
- Struis, R.P.W.J., Stucki, S., Wiedorn, M., 1996. A membrane reactor for methanol synthesis. J. Membr. Sci. 113, 93–100. https://doi.org/10.1016/0376-7388(95) 00222-7
- Studt, F., Behrens, M., Kunkes, E.L., Thomas, N., Zander, S., Tarasov, A., Schumann, J., Frei, E., Varley, J.B., Abild-Pedersen, F., Nørskov, J.K., Schlögl, R., 2015. The mechanism of CO and CO2 hydrogenation to methanol over Cu-based catalysts. ChemCatChem 7, 1105–1111. https://doi.org/10.1002/cctc.201500123.
- Takht Ravanchi, M., Kaghazchi, T., Kargari, A., 2009. Application of membrane separation processes in petrochemical industry: a review. Desalination 235, 199–244. https://doi.org/10.1016/j.desal.2007.10.042.
- Tameh, M.S., Dearden, A.K., Huang, C., 2018. Accuracy of density functional theory for predicting kinetics of methanol synthesis from CO and CO 2 hydrogenation on copper. J. Phys. Chem. C 122, 17942–17953. https://doi.org/10.1021/acs. jpcc.8b06498.
- Uemiya, S., 2004. Brief review of steam reforming using a metal membrane reactor. Top. Catal. 29, 79–84. https://doi.org/10.1023/b:toca.0000024930.45680.c7.
- van den Berg, R., Prieto, G., Korpershoek, G., van der Wal, L.I., van Bunningen, A.J., Lægsgaard-Jørgensen, S., de Jongh, P.E., de Jong, K.P., 2016. Structure sensitivity of Cu and CuZn catalysts relevant to industrial methanol synthesis. Nat. Commun. 7, 13057 https://doi.org/10.1038/ncomms13057.
- Van Tran, T., Le-Phuc, N., Nguyen, T.H., Dang, T.T., Ngo, P.T., Nguyen, D.A., 2018. Application of NaA membrane reactor for methanol synthesis in CO2 hydrogenation at low pressure. Int. J. Chem. React. Eng. 16, 1–7. https://doi.org/10.1515/ijcre-2017-0046.
- Zander, S., Kunkes, E.L., Schuster, M.E., Schumann, J., Weinberg, G., Teschner, D., Jacobsen, N., Schlögl, R., Behrens, M., 2013. The role of the oxide component in the development of copper composite catalysts for methanol synthesis. Angew. Chem. Int. Ed. 52, 6536-6540. https://doi.org/10.1002/anie.201301419.